BIOMIMETICS

Ladybird beetle–inspired compliant origami

Sang-Min Baek[1,2], Sojung Yim[1,2], Soo-Hwan Chae[1,2], Dae-Young Lee[1,2,3,4], Kyu-Jin Cho[1,2]*

Origami can enable structures that are compact and lightweight. The facets of an origami structure in traditional designs, however, are essentially nondeformable rigid plates. Therefore, implementing energy storage and robust self-locking in these structures can be challenging. We note that the intricately folded wings of a ladybird beetle can be deployed rapidly and effectively sustain aerodynamic forces during flight; these abilities originate from the geometry and deformation of a specialized vein in the wing of this insect. We report compliant origami inspired by the wing vein in ladybird beetles. The deformation and geometry of the compliant facet enables both large energy storage and self-locking in a single origami joint. On the basis of our compliant origami, we developed a deployable glider module for a multimodal robot. The glider module is compactly foldable, is rapidly deployable, and can effectively sustain aerodynamic forces. We also apply our compliant origami to enhance the energy storage capacity of the jumping mechanism in a jumping robot.

INTRODUCTION

The rapid deployment and load-bearing abilities of foldable wings enhance the versatility of the locomotion of flying and gliding animals (1–10). Rapid deployment of folded wings allows an animal to quickly change its locomotive mode from ground to aerial, thus enabling them to adapt to drastic environmental changes or predatory situations. The load-bearing ability of deployed wings ensures flight stability by preventing wing failure that could otherwise occur from the aerodynamic forces applied during flight. To achieve these properties, birds actively control their muscles and bones (3–5). Different from birds, insects have membranous wings that are boneless and without muscle; thus, they must use the strategically patterned compliant structures of their wings, specifically the wing's resilin and vein (6–10).

The resilin and the vein usually perform different tasks in insect behaviors. Resilin is located in various appendages of the insects, such as wings, legs, and jaws. Resilin is mainly in charge of the elastic energy storage, which enables rapid and vigorous motions, like jumping, which requires large power, far beyond the muscle output (11–17). The vein's main role is to support the insect's wings to keep the wings from being folded during flight (8, 9). In contrast to these examples, ladybird beetles have specialized veins that enable both rapid self-deploying and robust load-bearing capabilities (10). A ladybird beetle can deploy its intricately folded wings within 100 ms, and its wings can effectively sustain aerodynamic forces during high-frequency flapping. A key feature of this beetle's wing is the geometry and deformation of the wing frame, specifically, its tape-spring shaped vein. The veins' cross-sectional curvature and compliance render both elastic energy storage and self-locking abilities. The cross-sectional curvature induces high initial stiffness of the vein and enables self-locking of the wing. The vein's initially curved configuration flattens during wing folding, and large strain energy is stored on the vein. This large energy storage and the self-locking abilities of the vein form the core foundation of the ladybird beetle's rapid self-deployable and load bearing wings.

In synthetic systems, energy storage/release and structural locking techniques are also well-established methods for kinetic and static behavior design (18, 19). Especially in deployable systems, an analogy can be drawn between nature and synthetic systems; energy storage can facilitate the rapid transformations between the packed-and-stored state and the deployed-and-operating state, and the locking ability ensures reliable operation of the deployable system by maintaining the deployed configuration. The storable tubular extendible member (STEM), which uses elastic tape spring, is a representative case of these techniques and has been applied to the various systems (20–24). However, because of the absence of clearly defined joints, using complex kinematic behavior to the STEM or folding it flat is limited.

Origami is a longstanding solution for designing compact and lightweight deployable systems; it accomplishes complex kinematic behavior and flat folding easily by patterning flat rigid facets and defined fold lines. On the basis of these advantages, the origami-inspired design has been applied to the various scales of applications, such as locomotive robots (25–28), a shock-absorbing mechanism (29), metamaterials (30–32), self-assembly (33, 34), wearable robots (35), and soft robotics (36, 37). In addition, various analyses were performed to diversify origami-inspired designs (38–41). To extend the functionality of the origami structure, various attempts have been made to augment physical properties besides traditional geometric designs. However, embedding physical properties by attaching conventional mechanical components to the origami structure limits the core advantages of the origami, such as compact and lightweight properties. To address these limitations, origami design principles have been proposed in previous research (42–44). Kim et al. (42) presented a perpendicular folding principle to enhance the load-bearing ability of origami structures. Faber et al. (43) developed programmable three-dimensional (3D)–printed origami structures by designing flexure stiffness profiles. Mintchev et al. (44) presented a dual-stiffness origami structure based on prestretched elastic flexures.

Origami structure, using a compliant membrane as a fold-line material, usually uses a thin and narrow folding area as an energy-storing element, and also the locking ability of the origami structure relies on the structural configuration of multiple facets. Therefore, the energy storage capacity of the origami structure is limited and tends to be bulky to perform locking. However, foldable systems in nature, in particular ladybird beetle wings, perform both large energy storage and self-locking, with only a simple skeletal structure

[1]Soft Robotics Research Center, Seoul National University, Seoul, Republic of Korea. [2]Department of Mechanical and Aerospace Engineering, Institute of Advanced Machines and Design, Seoul National University, Seoul, Republic of Korea. [3]School of Engineering and Applied Sciences, Harvard University, Cambridge, MA, USA. [4]Wyss Institute for Biologically Inspired Engineering, Harvard University, Cambridge, MA, USA.
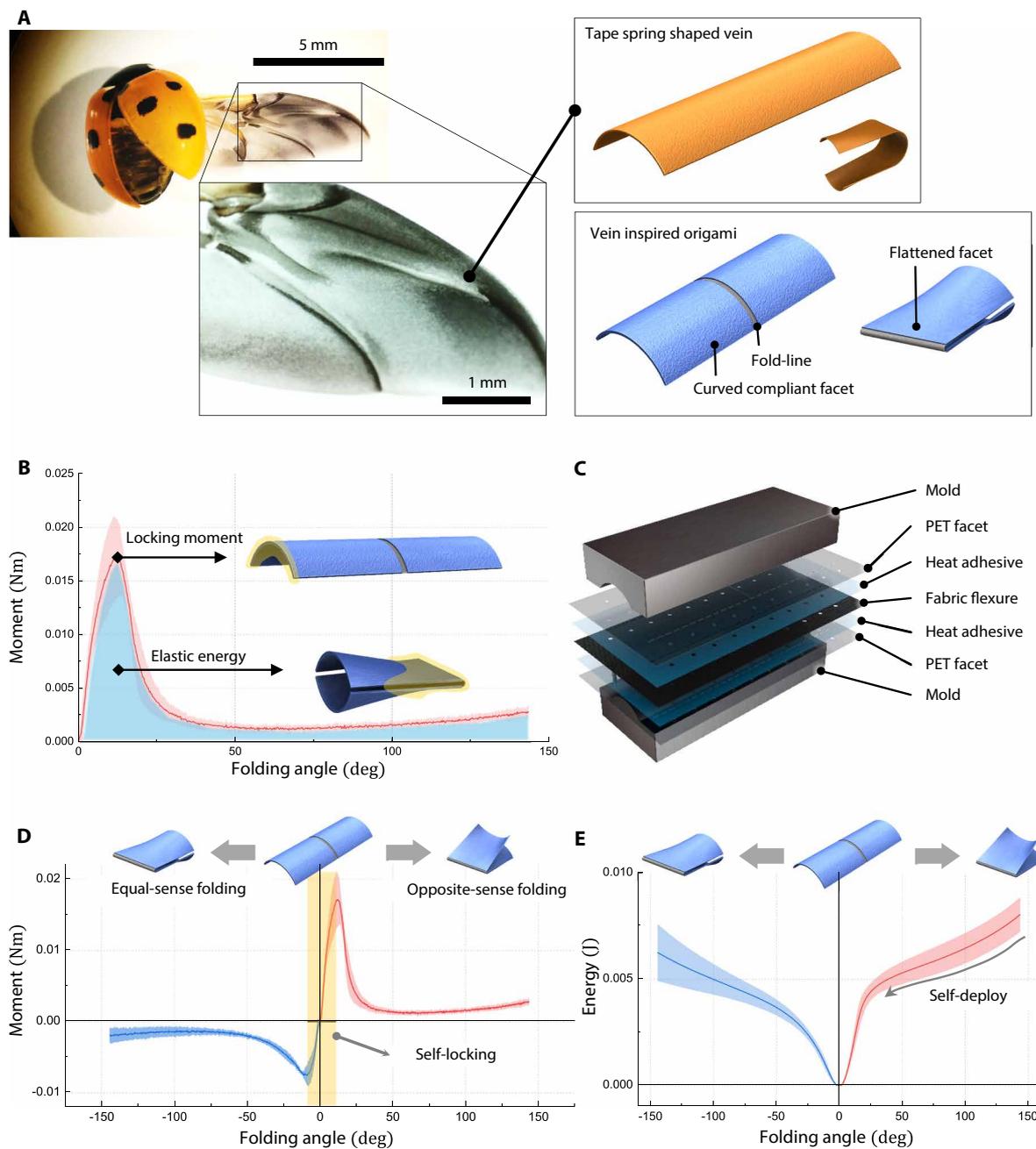*Corresponding author. Email: kjcho@snu.ac.kr

Fig. 1. Ladybird beetle–inspired compliant origami. (**A**) Ladybird beetle's wing vein and ladybird beetle–inspired compliant origami. The compliant origami is composed of compliant facets with a cross-sectional curvature. (**B**) Self-locking behavior of the compliant origami (red) and energy storage of the compliant origami (blue). (**C**) Fabrication of the compliant origami. Predesigned molds are applied. (**D**) Folding moment according to the folding angle. The compliant origami has an anisotropic moment profile. Two peak folding moments render the self-locking. (**E**) Stored energy according to the folding angle. This energy storage renders self-deployment of the compliant origami. The lines in (B), (D), and (E) represent the mean values, and the shaded regions represent ±1 SD.

(Fig. 1A). The limitations of synthetic systems arise from the rigidity assumption in origami design, which treats the facet as a flat, rigid, and nondeformable plate (45). Therefore, previous origami applications have focused on the flexure design to acquire deformation-related functionality in the origami structure, especially in the case of energy storage. However, the flexure, which undergoes high strain concentration in repeated folding and unfolding, must be made from a highly elastic material to prevent plastic deformation. Thus, the

flexure usually has a low Young's modulus (fig. S1 and note S1). In this design scenario, the energy storage is limited. Furthermore, the flexure is easily deformed by external loads. Thus, origami locking mechanisms mainly rely on multiple facets and their supporting components, such as magnets and springs, to prevent flexure deformation.

In this study, we aim to widen the programmable space of both kinetic and static behaviors of the origami by adopting principles of ladybird beetle wings (Movie 1). We propose the introduction of

Movie 1. Summary of labybird beetle–inspired compliant origami and its applications.

to produce curved facets, we used pre-designed molds in the heat laminating step (Fig. 1C and movie S1).

During folding of the compliant origami, the area of the curved facet near the fold line gradually flattens, and elastic energy is stored on the deformed facets (Fig. 1B). This stored energy enables the compliant origami to rapidly deploy within 116 ms. Furthermore, the curved geometry of the facet gives compliant origami the ability to self-lock. The proposed compliant origami can sustain 150 times its own weight (up to 210 g, moment arm of 45 mm) (movie S1 and fig. S2).

Ladybird beetle–inspired compliant origami

The proposed compliant origami has two main functionalities: self-locking (Fig. 1D) and energy storage (Fig. 1E). To validate these properties, we measured the folding moment according to the folding angle and calculated the stored energy from the moment data. An analytical model was also proposed to predict these properties (note S2). The lumped model, similar to the pseudo-rigid body model (50), assumes the curved compliant facet as four rigid plates and three torsion springs (Fig. 2A). The proposed model can predict the locking moment; however, it is limited in its ability to predict the energy storage. In the real-world case, during the folding, the flattened area of the curved facets gradually propagates away from the fold line; this propagation partially contributes the energy storage of the origami structure (fig. S3G). However, the proposed model cannot represent this propagation; thus, the model prediction of the stored energy is less accurate than the prediction of the moments.

We selected three design parameters: radius of curvature (r), arch length (w), and facet thickness (t) (Fig. 2A and table S1). The compliant origami with a radius of curvature of 12 mm, arch length of 20 mm, and facet thickness of 200 μm was set as a reference, and the experimental and analytical data were collected by changing each of the design parameters, while the other parameters were fixed as reference values.

Figure 1D shows the folding moment, and Fig. 1E shows the stored energy according to the folding angle of the reference design. The folding moment data show two characteristics: (i) the initial peak moment and (i) the anisotropic moment profile, which depends on the folding directions. The initial peak moment represents the load-bearing ability of the compliant origami. Therefore, the compliant origami performs as a self-locking mechanism in the region between the two peak moments. Also, the energy is stored on the facets; this energy enables the rapidly self-deployable feature of the compliant origami. The compliant origami shows different behaviors depending on the folding directions, which are equal-sense folding and opposite-sense folding. Opposite-sense folding has a higher peak moment, meaning the self-locking ability is better when the folding is in the opposite-sense direction. The energy storage capacity is also better when opposite-sense folding is used; however, the difference in the peak moment between the two folding directions is greater than that of the energy storage capacity.
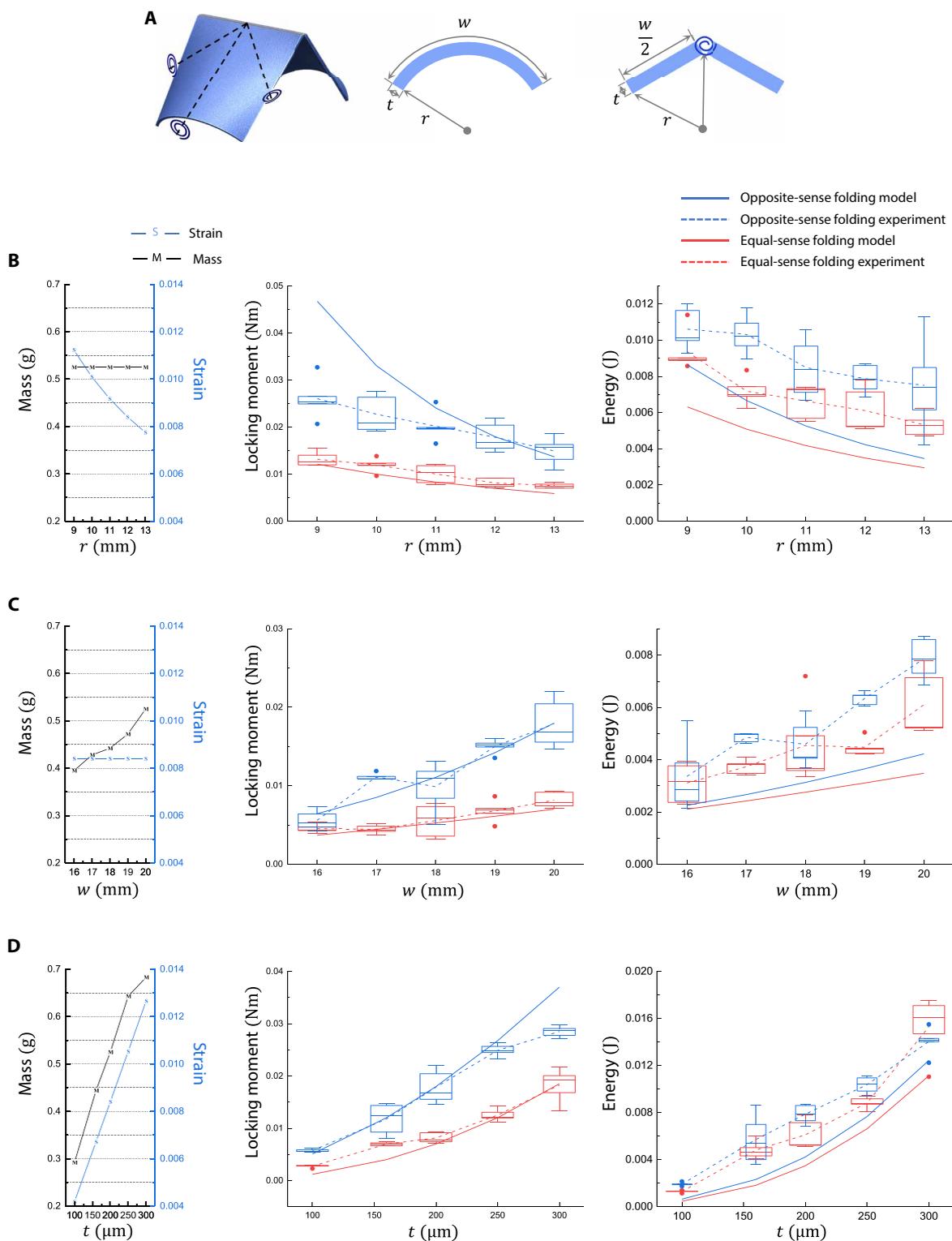
deformation of the facet into the origami design not only to enhance its self-locking ability in its initial configuration but also to enable rapid self-deployment by elastic energy storage (Fig. 1A). Our origami structure is composed of compliant facets with cross-sectional curvature, as conceptualized in previous research (46). A high second moment of area of the initially curved facets is proposed to enable a high self-locking moment. Flattening of the compliant facets in the folding is used to enable large energy storage (Fig. 1B). In the folding and unfolding, the strain of the facets is lower than that of the flexures. Therefore, the facets can use materials that are more than 100-fold stiffer than those of flexures (fig. S1 and note S1) (47). As a result, stronger self-locking and large energy storage can be simultaneously addressed in a single origami joint without any additional components. To validate our design, we applied the ladybird beetle–inspired compliant origami to two robotic applications. First, we developed a deployable glider module for a multimodal robot. The glider module uses a high area reduction mechanism through its wing folding, and it deploys its wings rapidly by using the stored elastic energy of the origami facets. By strategically layering multiple origami structures, the glider wing could effectively sustain the aerodynamic forces applied during flight. Second, we developed a jumping mechanism based on origami. The proposed compliant origami design was applied to a flea-inspired jumper developed by Koh et al. (48). Without any additional mechanical components or any increase in the total weight of the jumper, energy storage was increased by introducing curvature and compliance to the facets.

RESULTS

The wing vein of a ladybird beetle serves as the main wing frame. Its primary features include compliance and a cross-sectional curvature; these features are applied to facets of the origami structure (Fig. 1A). The compliant origami is composed of polyethylene terephthalate (PET) facets and a rip-stop fabric flexure. The facets with compliance and curvature sandwich both sides of the flexure (movie S1). The fabrication processes are the same as those for the planar-based smart composite microstructure (SCM) fabrication process outlined in (49): fold-line cutting, heat laminating, and outline cutting. However,

Fig. 2. Performance study of the compliant origami. (**A**) Design parameters (radius of curvature *r*, arch length *w*, and facet thickness *t*) of the compliant origami. The analytical model assumes the curved facet as four rigid plates and three torsion springs. (**B**) (Left) Mass and strain of the compliant origami depending on *r* (blue denotes strain and black denotes mass). The (middle) locking moment and (right) energy storage of the compliant origami depending on *r* (blue denotes opposite-sense folding and red denotes equal-sense folding). (**C**) Mass and strain of the compliant origami depending on *w*. The locking moment and energy storage of the compliant origami depending on *w*. (**D**) Mass and strain of the compliant origami depending on *t*. The locking moment and energy storage of the compliant origami depending on *t*. Whiskers are extended to 1.5 times of interquartile range (IQR) from the edge of the box; IQR is the difference between upper and lower quartile. Solid circles indicate outliers that are beyond the whiskers.

Figure 2 (B to D) shows mass, maximum strain, locking moment, and stored energy, depending on the design parameters. A decrease of the radius of curvature increases both the locking moment and the stored energy while keeping the mass constant; this is because a more curved facet requires a larger deformation to be flattened. An increase of the arch length increases both the locking moment and the stored energy while keeping the maximum strain constant. This is because the wider arch length requires the deformation of a larger area of the facet. An increase of the thickness increases both the locking moment and the stored energy; it also increases both the mass and maximum strain because the increase of the facet's thickness increases facet stiffness. To target certain level of performance, at first, we roughly set the performance by selecting the facet thickness. Next, the radius of the curvature or the arch length is fine-tuned, depending on the important value (mass or strain) of the target. Further analysis about the deployment time and scalability of the compliant facet is described in the Supplementary Materials (notes S3 and S4).

Deployable glider module

Gliding enables energy-efficient, multimodal locomotion of various animals and locomotive robots by using potential energy (51–55). There are several requirements for a glider to perform multimodal locomotion. Specifically, the glider should not hinder the other locomotion performance, transitions between locomotive modes should be rapid, and the gliding should be robust (55). Therefore, the glider should be lightweight, foldable, and rapidly deployable, and the glider should have load-bearing ability. To address these requirements, we developed a deployable glider module based on the compliant origami frame. The glider module weighs 35 g without electronics, its wing span is 660 mm, and it can be compactly folded into one-eighth of its deployed area (Fig. 3A).

Normally, there's a tradeoff in design between load bearing and ease of compact folding. Compact folding usually requires multiple fold lines and complex folding patterns; however, it reduces load-bearing ability. Likewise, a design with a high load-bearing ability typically means that more force is required to transform the origami structure to the folded mode. Overcoming this tradeoff is a main challenge of this application. To address this challenge, we used the kinematic relation of strategically double-layered compliant origami structures (Fig. 3C). Each side of the wing is composed of double layers of compliant origami structures. Each origami structure consists of two facets and a single fold line. These two origami structures overlap each other (one above the other), and the fold lines of each origami structure are offset (Fig. 3C). In addition, one end of the overlapped origami layers, which becomes a proximal part of the whole glider, is connected to the body by pin joints (Fig. 3C). Thus, the transverse folding of the origami frame is coupled with a rotation of the pin joints, which is shoulder folding. As a result, the wing can be compactly folded into one-eighth of the deployed area. The kinematic relation of the overlapped origami layers makes folding in the $-x$ direction easy and folding in the x direction hard (Fig. 3D). Therefore, the origami frame is arranged to endure aerodynamic forces in the x direction and mode-changing folding in the $-x$ direction. We performed experiments to validate how much moment the wing frame can sustain and how much moment is required to fold the wing. The results show that the origami wing frame can sustain six times the moment required to fold the glider (Fig. 3D). This means that the glider is easily foldable but can effectively sustain aerodynamic

forces in its deployed state. This difference between the locking moment and the folding moment is larger than the difference observed between equal-sense folding and opposite-sense folding (Fig. 1D). The reason is that the origami wing frame kinematically has no degree of freedom in the load-bearing direction. Thus, the folding in origami joint is blocked, and the bending occurs in the curved facet, when load exceeding threshold is applied. This is similar to the bending of a tape spring, which has higher load-bearing ability than an origami joint (20).

Folding of the glider is actuated by a winding motor with a wire-driven mechanism with a crown gear clutch (note S5 and fig. S6). Self-deployment is triggered by a trigger motor, which actively attaches and detaches the connection between the winding motor and the wing. When the trigger motor detaches the connection, the folded glider deploys rapidly (within 466 ms) by using the energy stored on the compliant origami frames (Fig. 3E).

As a result, the glider module with three features (easily compact-foldable, rapidly self-deployable, and robust self-locking in deployed state) was developed and integrated with a jumping mechanism to show the multimodal locomotion capability (Fig. 3B and movie S2). Ease of compact folding allowed the use of lightweight folding actuation, which, in turn, makes the whole glider light. This lightness and compact foldability minimize the hindrance to the jumping locomotion. The rapid self-deployment makes the transition of locomotion from jumping to the gliding fast. These reductions in jumping performance hindrance and transition time ensure that the robot can start to glide in higher apex; therefore, the robot can travel further with energy efficiency. Furthermore, self-locking of the glider prevents wing failure by effectively sustaining the aerodynamic forces that lift the whole weight of the robot, including the jumping mechanism.

The proposed deployable glider module was also applied to the crawl-gliding robot and flapping mechanism to show applicability on various locomotive robots (movies S3 and S4 and notes S6 and S7). The crawl-gliding robot could crawl effectively on the ground in a wing-folded configuration, and it could deploy its wings and glide when the robot fell from the cliff. The gliding ensures the safe landing of the robot, and it also increases the travel distance of the robot. We developed a deployable flapping mechanism by applying a rotating crank four-bar mechanism to the deployable glider module. The deployable flapping mechanism could be folded in a confined space and easily transported. When the robot needs to fly, it deploys its wings and starts flapping. During flapping, the compliant origami frames let the wings effectively sustain aerodynamic forces required for flying.

Origami-based jumping mechanism

In nature, jumping is performed by small creatures to overcome relatively large obstacles or to rapidly escape from predatory situations (56, 57). The core mechanisms of jumping locomotion are storing a large enough amount of energy to propel the body, while overcoming gravity, and enlarging output power by rapidly releasing the stored energy (56). Inspired by these characteristics, various high-performance jumping robots have been developed (58–62). Previously developed jumping robots were composed of a spring-actuator system for energy storage and a linkage system to transmit force to the ground. In these systems, the energy storage component must propel the whole mass, including the linkage system, which does not have any energy storage capacity. Unlike these synthetic systems, the exoskeletons of locust's legs, which are akin to the linkages of a robot, do have energy
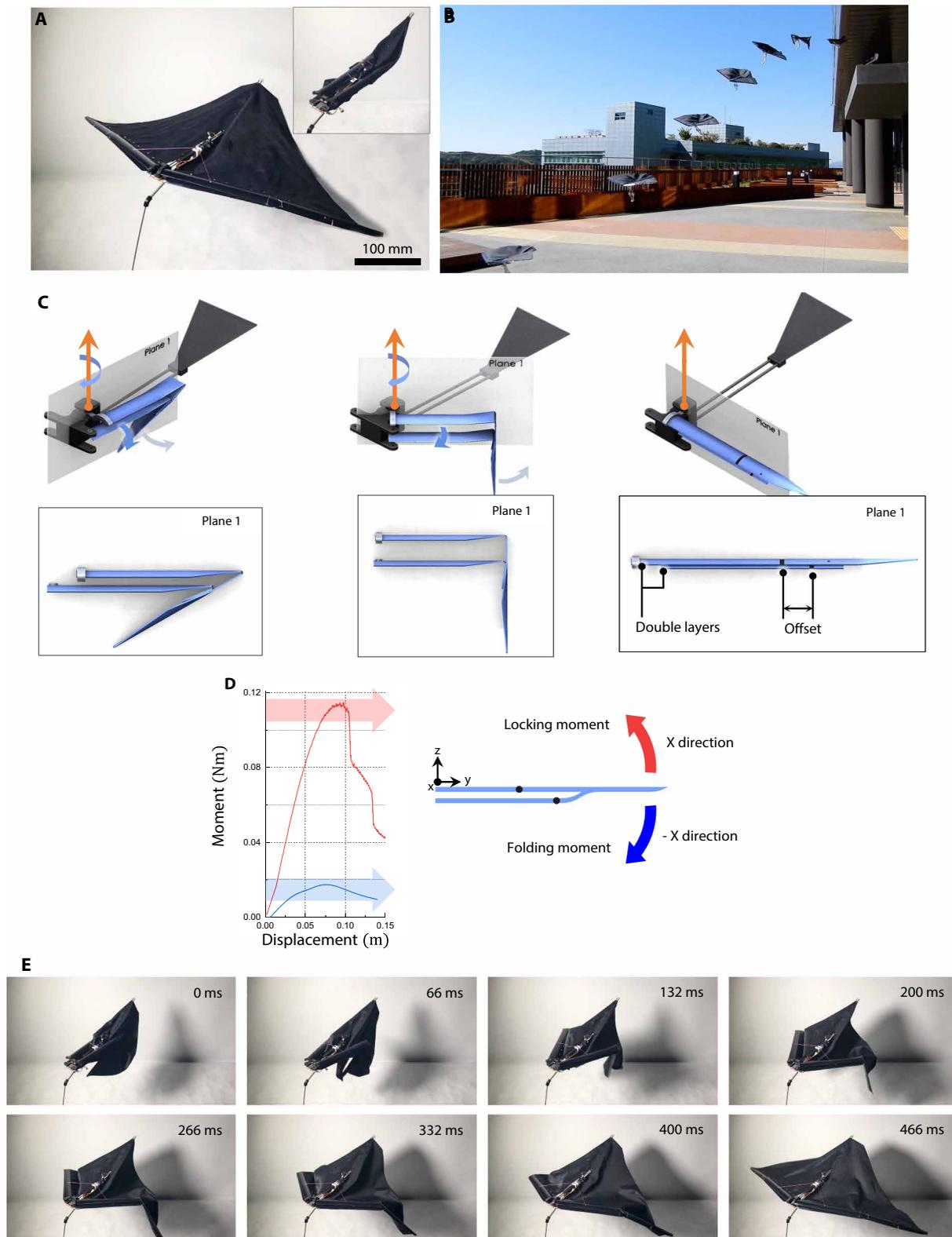
Fig. 3. Deployable glider module. (**A**) The deployable glider module can be folded into one-eighth of its deployed area. (**B**) The glider module was integrated with a jumping mechanism, and the jump-gliding robot was tested outdoors. (**C**) Kinematic design of the wing folding and unfolding mechanism. Two compliant origami frames were strategically arranged to enlarge the load-bearing ability. (**D**) Moment required to transform the wing in the folded state (blue) and locking moment that the wing can sustain (red). The solid lines represent the mean values, and the shaded regions represent ±1 SD. (**E**) Sequence of the deployment. The glider can deploy within 466 ms by using the stored energy in the compliant origami.
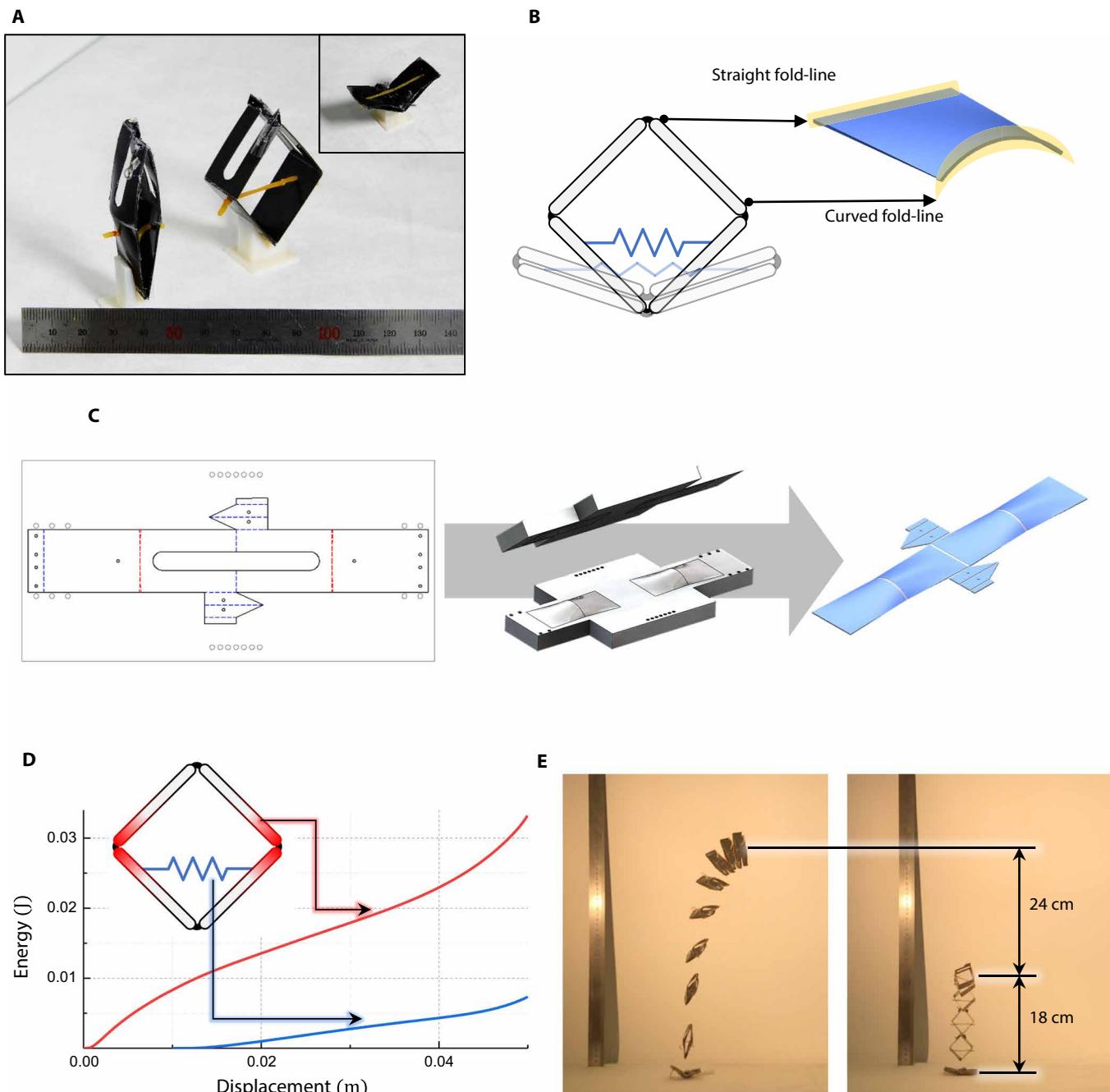
Fig. 4. Origami-based jumping mechanism. (**A**) Flea-inspired jumping mechanisms. The left one contains compliant origami, and the right one is composed of conventional origami linkages. (**B**) Unique shape of the origami facet. Each side of the jumper consists of compliant origami joints; the top and bottom sides consist of a conventional origami joint. (**C**) Fabrication of the jumping mechanism based on compliant origami. On the planar drawing, red indicates curved fold lines and blue indicates straight fold lines. An origami structure with combined joints is fabricated by predesigned molds in a single SCM process. (**D**) Energy storage of the jumper by compliant origami (red) and linear spring (blue). (**E**) Jumping performance of two origami-based jumping mechanisms. The left jumper with compliant origami jumps 42 cm, and right jumper without compliant origami jumps 18 cm.

storage capacity. This energy supports 40% of the jumping performance (63, 64). This shows how the skeletal structure supports and maximizes the energy storage in nature; this is very similar to the ladybird beetle's wing vein, which is a wing frame structure that also enables rapid deployment of a folded wing by using stored energy. Like these insects, we focused on enlarging the energy storage of the jumping mechanism. We benchmarked a flea-inspired jumper

developed by Koh *et al.* (*48*) and applied our proposed compliant origami design method (Fig. 4A).

The flea-inspired jumper is composed of a rhombus-shaped, closed-chain, four-bar origami linkage, a linear spring for energy storage, and a shape memory alloy (SMA) spring for triggering (fig. S7). The linear spring was horizontally installed on the center of the linkage, and the trigger SMA was installed on the stopper structure,

which is on the top of the linkage. The key principle of jumping is the torque reversal catapult mechanism (note S8). To enlarge energy storage, we strategically applied compliant origami design on the appropriate joints of the jumping mechanism. The jumping mechanism has two states: energy-stored state and energy-released state. In the stored state, the rhombus-shaped four-bar linkage is flattened laterally—namely, two joints on the sides are flexed. In the released state, on the other hand, the linkage is flattened vertically—namely, two joints on the top and bottom are flexed. On the basis of these kinematic configurations of the jumping mechanism, we applied proposed compliant origami to joints on each side of the linkage, which were folded in an energy-stored state. On the other hand, two joints on the top and bottom were designed as conventional origami joints to maintain the kinematic configuration of energy released state. Therefore, a unique-shaped facet was designed that joined continuously from the curved fold line to the straight fold line (Fig. 4B). To fabricate this origami structure, we used predesigned molds in the heat laminating step. As a result, a selectively curved origami structure that has selectively patterned joint stiffness was fabricated in a single SCM fabrication process (Fig. 4C).

On the basis of the compliant origami design, the stored energy of the jumper is enlarged (Fig. 4D); this is similar to installing a torsion spring in the joints on both sides of the linkage, but without any weight increase. We fabricated two different jumpers (Fig. 4A)—one with our design method and the other without our design method. Except for the curvature on the facet, the other design parameters are identical in the two jumpers. From the experiments, the modified mechanism was shown to jump 133% more than the original jumper (Fig. 4E and movie S5).

DISCUSSION

In this study, we developed a compliant origami structure, inspired by ladybird beetles, that rapidly deploys within 116 ms and can bear loads up to 210 g (150 times its own weight). We achieved large energy storage and robust self-locking abilities in our structure by deviating from traditional origami design. From the experiments and the analytical model suggested in this manuscript, the energy storage and self-locking abilities of the compliant origami can be engineered. In addition, we applied the compliant origami into two robotic applications: a deployable glider module and an origami jumping mechanism. The results showed that introducing the compliant origami enhances both the kinetic and the static behavior of the robotic systems.

Our work also enables the integration of compliant origami into complex origami structures. By tailoring the proposed origami design into an origami-based structure with multiple fold lines, the structural characteristics could be designed without additional components. The proposed robotic applications present a few of these examples. The deployable glider module uses a kinematic relation of the double-layered origami frames whose joints are offset to each other to increase the locking performance and deployment speed while maintaining ease of folding. In the origami jumping mechanism, the compliant origami design is applied to selective joints of the four-bar linkage, to distinguish energy stored and released states, while enlarging the energy density of the jumping mechanism. In addition, the proposed facet design principle is applied to a Miura-ori pattern to show effects of the tailoring the compliant origami into the complex origami structures and the scalability of the fabrication

process (note S9 and movie S6). Also, the scaling effect in design is considered on the basis of the proposed analytical model (note S4). The structural functionality of the origami can be established by strategically applying the proposed compliant origami to selective joints of the origami structure.

Our proposed compliant origami does have some limitations that require further study. In this work, only the arch shape was considered as the facet geometry and PET as the material. Therefore, future work should also consider the effects of various facet geometries and different facet materials. There are also several points to be further dealt with in the proposed robotic applications. The deployable glider module was manually controlled by using a radio controller. After jumping, the operator commanded the glider module to deploy its folded wings around peak height. However, for effective multimodal locomotion, the timing of the wing deployment is an important consideration in locomotion performance because it affects the transition phase and the aerodynamics of the jump-gliding locomotion. For even greater robotic autonomy, the gliding trajectory and direction should be controlled; one possible solution could be to generate a moment on to the whole robot by relative motion between the jumper and the glider. In the jump-gliding robot, the jumper was attached to the glider module by a revolute joint, and the relative rotation between the jumper and the glider regulates the distance between the center of mass and the center of pressure, which generates a moment on the whole robot to control the gliding trajectory and direction.

The proposed origami jumping mechanism was only focused on the enlargement of the energy storage. For the active energy storing, however, the required force for energy storing should also be considered and an appropriate actuator should be selected. The choice of actuator (considering weight and maximum output force) will affect the design of the compliant origami joints and the jumpers' performance. To effectively jump, the energy storage should be maximized while using a lightweight actuator, which usually has a low force limit. Therefore, a force profile optimization of the energy storing mechanism, which can be obtained by combining the compliant origami and linear spring, is required.

MATERIALS AND METHODS
Fabrication

The fabrication process is the same as those outlined for a planar-based SCM process (49), specifically fold-line cutting, heat laminating, and outline cutting. However, to produce curved facets, we used predesigned aluminum molds in the heat laminating step (Fig. 1C and movie S1). PET film (COSBIG) with preapplied heat adhesive on a single side was selected for the facets (thickness of reference design is 0.2 mm), and rip-stop fabric (thickness of 0.1 mm; ARO Tech) was selected for the flexures. The molds were used for thermoforming the facets into the target curved shape in the heat laminating step. Thus, the molds have a predesigned curved shape in the contact area. The molds are composed of two parts: concave and convex. To align the molds and films, the molds have pin holes. The following outlines the detailed fabrication steps:

1) Laser-cut (VLS 3.50, Universal Laser System) the fold-line patterns and alignment pin holes on two PET films.

2) Laser-cut the pattern and the alignment pin holes on rip-stop fabric.

3) Layer the rip-stop fabric in between the PET films.

4) Place the sandwiched films in between the molds and align the patterns by using the pin holes and pins.

5) Heat press (QM900A, QME-SYS) the sandwiched molds with films in 110°C and 1 MPa for 5 min; this step melts the heat adhesives and deforms the PET into the target curved shape.

6) Cool down at room temperature while maintaining the pressure and then disassemble the molds and release the laminate from the molds and pins.

7) Cut outlines of the laminated structure.

The deployable glider module is composed of a compliant origami wing frame (radius of curvature of 12 mm, arch length of 20 mm, and thickness of 300 μm), 3D-printed body parts [acrylonitrile butadiene styrene (ABS)–like material, Cubicon Lux Full HD, Cubicon], a carbon fiber rod body frame (diameter of 2 mm), and two motors for wing folding and unfolding (winding motor: 700:1 geared DC motor, LCP06-A03V-0700, D&J WITH Co. Ltd. and trigger motor: 136:1 geared DC motor, LCP06-A03V-0136, D&J WITH Co. Ltd.).

The jumping mechanism is composed of an origami linkage (radius of curvature of 12 mm, arch length of 20 mm, and thickness of 500 μm), a triggering SMA (diameter 0.20 mm, 70°C Flexinol Actuator Wire, DYNALLOY Inc.), and a linear spring (rubber band).

Experiments

To study the performance of the origami structure, we selected three design parameters: radius of curvature, arch length, and facet thickness. Each parameter was tested for five different values, whereas other parameters were fixed at reference values (radius of curvature of 12 mm, arch length of 20 mm, and thickness of 200 μm). Thus, a total of 13 designs were prepared (table S1). To measure the folding moment, we assembled each specimen to the rotational actuator (Dynamixel MX-28T, Robotis) using a 3D-printed connector (VeroWhitePlus, Objet 260, Stratasys). The connector was designed to align the specimen's fold line to the actuator's center of rotation. While rotating the specimen, the other side of the specimen pressed the load cell (KTOYO 333FB, 1 kgf) and was folded. The rotating angle versus force data were collected (NI Compact DAQ, NI 9237, National Instruments) (fig. S9A).

Wing loading and folding moments were measured by load cell (models UMM-G200 and UMM-G500, Dacell) and with a universal testing machine (model RB302, R&B). The wing frame specimen was mounted on the test bed using a 3D-printed holder (VeroWhitePlus, Objet 260, Stratasys). To measure the wing folding moment, a wire fixed on the wing tip was pulled in the wing folding direction by the testing machine; the load cell (model UMM-G200, Dacell) measured tension on the wire according to the pulled distance. To measure the wing loading moment, a pin connected on the testing machine pushed the wing frame in a wing loading direction, and the load cell (model UMM-G500, Dacell) measured applied force on the pin according to the pushed distance. The objective of these experiments was to quantify the peak moment, so the data were collected until a few seconds after the peak force values appeared (fig. S9B).

Jumping energy was measured by load cell (models UMM-G200 and UMM-G500, Dacell) and by a universal testing machine (model RB302, R&B). Initially, the top of the jumper was compressed in a flat configuration by the load cell, which was connected to the testing machine. Next, the testing machine slowly released the compressed jumper until it returned to its unloaded original configuration; the load cell (model UMM-G200 for normal jumper and model UMM-G500 for curved jumper, Dacell) measured the force applied by the jumper (fig. S9C).

SUPPLEMENTARY MATERIALS

robotics.sciencemag.org/cgi/content/full/5/41/eaaz6262/DC1
Note S1. Differences between conventional origami and compliant origami.
Note S2. Analytical model for the compliant origami.
Note S3. Deployment time and average deployment speed of the compliant origami.
Note S4. Scale effect of the compliant origami.
Note S5. Wing folding and unfolding mechanism of the deployable glider module.
Note S6. Crawl-gliding locomotion.
Note S7. Deployable flapping mechanism based on the ladybird beetle–inspired compliant origami.
Note S8. Flea-inspired jumping mechanism and torque reversal catapult mechanism.
Note S9. Miura-ori pattern with compliant origami design.
Fig. S1. Possible materials for the fold line of the conventional origami and for the facet of the compliant origami.
Fig. S2. Self-locking and self-deployment of the compliant origami.
Fig. S3. Analytical model for the compliant origami.
Fig. S4. Deployment time and average deployment speed of the compliant origami.
Fig. S5. Scale effect of the compliant origami.
Fig. S6. Wing folding and unfolding mechanism of the deployable glider module.
Fig. S7. Flea-inspired jumping mechanism and torque reversal catapult mechanism.
Fig. S8. Miura-ori pattern with compliant origami design.
Fig. S9. Experimental setups.
Table S1. Variables for the compliant origami.
Table S2. Denavit-Hartenberg parameters for the analytical model.
Movie S1. Ladybird beetle–inspired compliant origami.
Movie S2. Deployable glider module for jump gliding.
Movie S3. Deployable glider module for crawl gliding.
Movie S4. Deployable flapping mechanism.
Movie S5. Origami-based jumping mechanism.
Movie S6. Miura-ori pattern with compliant origami design.

REFERENCES AND NOTES

1. K. Stowers, L. Y. Matloff, D. Lentink, How pigeons couple three-dimensional elbow and wrist motion to morph their wings. *J. R. Soc. Interface* **14**, 20170224 (2017).
2. D. Lentink, U. K. Müller, E. J. Stamhuis, R. de Kat, W. van Gestel, L. L. M. Veldhuis, P. Henningsson, A. Hedenström, J. J. Videler, J. L. van Leeuwen, How swifts control their glide performance with morphing wings. *Nature* **446**, 1082–1085 (2007).
3. R. A. Meyers, E. F. Stakebake, Anatomy and histochemistry of spread-wing posture in birds. 3. Immunohistochemistry of flight muscles and the "shoulder lock" in albatrosse. *J. Morphol.* **263**, 12–29 (2005).
4. R. L. Nudds, G. J. Dyke, J. M. V. Rayner, Avian brachial index and wing kinematics: Putting movement back into bones. *J. Zool.* **272**, 218–226 (2007).
5. M. Di Luca, S. Mintchev, G. Heitz, F. Noca, D. Floreano, Bioinspired morphing wings for extended flight envelope and roll control of small drones. *Interface Focus* **7**, 20160092 (2017).
6. F. Haas, J. Kukalová-Peck, Dermaptera hindwing structure and folding: New evidence for familial, ordinal and superordinal relationships within Neoptera (Insecta). *Eur. J. Entomol.* **98**, 1375–1381 (2001).
7. F. Haas, S. Gorb, R. J. Wootton, Elastic joints in dermapteran hind wings: Materials and wing folding. *Arthropod Struct. Dev.* **29**, 137–146 (2000).
8. F. Hass, S. Gorb, R. Blickhan, The function of resilin in beetle wings. *Proc. R. Soc. Lond. B* **267**, 1375–1381 (2000).
9. K. Saito, S. Yamamoto, M. Maruyama, Y. Okabe, Asymmetric hindwing foldings in rove beetles. *Proc. Natl. Acad. Sci. U.S.A.* **111**, 16349–16352 (2014).
10. K. Saito, S. Nomura, S. Yamamoto, R. Niiyama, Y. Okabe, Investigation of hindwing folding in ladybird beetles by artificial elytron transplantation and microcomputed tomography. *Proc. Natl. Acad. Sci. U.S.A.* **114**, 5624–5628 (2017).
11. M. Kovač, The bioinspiration design paradigm: A perspective for soft robotics. *Soft Robot.* **1**, 28–37 (2014).
12. S. N. Gorb, Serial elastic elements in the damselfly wing: Mobile vein joints contain resilin. *Naturwissenschaften* **86**, 552–555 (1999).
13. W. Gronenberg, Fast actions in small animals: Springs and click mechanisms. *J. Comp. Physiol. A* **178**, 727–734 (1996).
14. H. C. Bennet-Clark, E. C. A. Lucey, The jump of the flea: A study of the energetics and a model of the mechanism. *J. Exp. Biol.* **47**, 59–76 (1967).
15. M. Rothschild, J. Schlein, K. Parker, C. Neville, S. Sternberg, The jumping mechanism of *Xenopsylla cheopis*. III. Execution of the jump and activity. *Philos. Trans. R. Soc. B Biol. Sci.* **271**, 499–515 (1975).

16. M. Burrows, G. P. Sutton, Locusts use a composite of resilin and hard cuticle as an energy store for jumping and kicking. *J. Exp. Biol.* **215**, 3501–3512 (2012).

17. S. N. Gorb, The jumping mechanism of cicada *Cercopis vulnerata* (Auchenorrhyncha, Cercopidae): Skeleton–muscle organisation, frictional surfaces, and inverse-kinematic model of leg movements. *Arthropod Struct. Dev.* **33**, 201–220 (2004).

18. D. Paluska, H. Herr, The effect of series elasticity on actuator power and work output: Implications for robotic and prosthetic joint design. *Robot. Auton. Syst.* **54**, 667–673 (2006).

19. M. Plooij, G. Mathijssen, P. Cherelle, D. Lefeber, B. Vanderborght, Lock your robot: A review of locking devices in robotics. *IEEE Robot. Autom. Mag.* **22**, 106–117 (2015).

20. K. Kwok, S. Pellegrino, Folding, stowage, and deployment of viscoelastic tape springs. *AIAA J.* **51**, 1908–1918 (2013).

21. Ö. Soykasap, S. Pellegrino, P. Howard, M. Notter, Folding large antenna tape spring. *J. Spacecr. Rockets* **45**, 560–567 (2008).

22. A. G. Tibert, S. Pellegrino, Deployable tensegrity masts, in *Proceedings of the 44th AIAA/ASME/ASCE/AHS/ASC Structures, Structural Dynamics, and Materials Conference*, Norfolk, VA, 7 to 10 April 2003 (American Institute of Aeronautics and Astronautics, 2003), p. AIAA-2013-1978.

23. S. Seriani, P. Gallina, A storable tubular extendible member (STEM) parallel robot: Modelization and evaluation. *Mech. Mach. Theory* **90**, 95–107 (2015).

24. L. Blanchard, G. Aridon, F. Falzon, D. Rémond, R. Dufour, A tape-spring hexapod for deployable telescopes: Dynamics, in *Proceedings of the International Conference on Space Optics* (SPIE), Noordwijk, Netherlands, 27 to 30 June 2006 (International Society for Optics and Photonics, 2006), p. 1056718.

25. A. Firouzeh, J. Paik, Robogami: A fully integrated low-profile robotic origami. *J. Mech. Robot.* **7**, 021009 (2015).

26. J.-S. Koh, K.-J. Cho, Omega-shaped inchworm-inspired crawling robot with large-index-and-pitch (LIP) SMA spring actuators. *IEEE/ASME Trans. Mechatron.* **18**, 419–429 (2013).

27. Z. Zhakypov, K. Mori, K. Hosoda, J. Paik, Designing minimal and scalable insect-inspired multi-locomotion millirobots. *Nature* **571**, 381–386 (2019).

28. D.-Y. Lee, S.-R. Kim, J.-S. Kim, J.-J. Park, K.-J. Cho, Origami wheel transformer: A variable-diameter wheel drive robot using an origami structure. *Soft Robot.* **4**, 163–180 (2017).

29. P. Sareh, P. Chermprayong, M. Emmanuelli, H. Nadeem, M. Kovac, Rotorigami: A rotary origami protective system for robotic rotorcraft. *Sci. Robot.* **3**, eaah5228 (2018).

30. J. L. Silverberg, A. A. Evans, L. McLeod, R. C. Hayward, T. Hull, C. D. Santangelo, I. Cohen, Using origami design principles to fold reprogrammable mechanical metamaterials. *Science* **345**, 647–650 (2014).

31. H. Fang, S.-C. A. Chu, Y. Xia, K.-W. Wang, Programmable self-locking origami mechanical metamaterials. *Adv. Mater.* **30**, e1706311 (2018).

32. E. T. Filipov, T. Tachi, G. H. Paulino, D. A. Weitz, Origami tubes assembled into stiff, yet reconfigurable structures and metamaterials. *Proc. Natl. Acad. Sci. U.S.A.* **112**, 12321–12326 (2015).

33. S. Felton, M. Tolley, E. Demaine, D. Rus, R. Wood, A method for building self-folding machines. *Science* **345**, 644–646 (2014).

34. S. Miyashita, S. Guitron, S. Li, D. Rus, Robotic metamorphosis by origami exoskeletons. *Sci. Robot.* **2**, eaao4369 (2017).

35. M. B. Oliveira, C. Liu, M. Zhao, S. M. Felton, Design of a variable stiffness wrist brace with an origami structural element, in *Proceedings of the ASME 2018 Conference on Smart Materials, Adaptive Structures and Intelligent Systems*, San Antonio, TX, 10 to 12 September 2018 (American Society of Mechanical Engineers, 2018), p. V002T08A009.

36. W. Kim, J. Byun, J.-K. Kim, W.-Y. Choi, K. Jakobsen, J. Jakobsen, D.-Y. Lee, K.-J. Cho, Bioinspired dual-morphing stretchable origami. *Sci. Robot.* **4**, eaay3493 (2019).

37. S. Li, D. M. Vogt, D. Rus, R. J. Wood, Fluid-driven origami-inspired artificial muscles. *Proc. Natl. Acad. Sci. U.S.A.* **114**, 13132–13137 (2017).

38. P. Sareh, thesis, University of Cambridge, Cambridge, UK (2014).

39. E. Rivas-Adrover, A new hybrid type of deployable structure: Origami-scissor hinged. *J. Int. Assoc. Shell Spat. Struct.* **59**, 183–190 (2018).

40. E. D. Demaine, M. L. Demaine, D. A. Huffman, D. Koschitz, T. Tachi, in *Origami 6*, K. Miura, T. Kawasaki, T. Tachi, R. Uehara, R. J. Lang, P. Wang-Iverson, Eds. (American Mathematical Society, 2015), pp. 209–230.

41. Y. Chen, R. Peng, Z. You, Origami of thick panels. *Science* **349**, 396–400 (2015).

42. S.-J. Kim, D.-Y. Lee, G.-P. Jung, K.-J. Cho, An origami-inspired, self-locking robotic arm that can be folded flat. *Sci. Robot.* **3**, eaar2915 (2018).

43. J. A. Faber, A. F. Arrieta, A. R. Studart, Bioinspired spring origami. *Science* **359**, 1386–1391 (2018).

44. S. Mintchev, J. Shintake, D. Floreano, Bioinspired dual-stiffness origami. *Sci. Robot.* **3**, eaau0275 (2018).

45. R. J. Lang, *Origami 4* (CRC Press, 2009).

46. S.-M. Baek, D.-Y. Lee, K.-J. Cho, Curved compliant facet origami-based self-deployable gliding wing module for jump-gliding, in *Proceedings of the ASME 2016 International Design Engineering Technical Conferences and Computers and Information in Engineering Conference*, Charlotte, NC, 21 to 24 August 2016 (American Society of Mechanical Engineers, 2016), p. V05BT07A028.

47. M. F. Ashby, *Materials Selection in Mechanical Design* (Butterworth-Heinemann, ed. 3, 2005).

48. J.-S. Koh, S.-P. Jung, M. Noh, S.-W. Kim, K.-J. Cho, Flea inspired catapult mechanism with active energy storage and release for small scale jumping robot, in *Proceedings of the 2013 IEEE International Conference on Robotics and Automation*, Karlsruhe, Germany, 6 to 10 May 2013 (IEEE, 2013), pp. 26–31.

49. R. J. Wood, S. Avadhanula, R. Sahai, E. Steltz, R. S. Fearing, Microrobot design using fiber reinforced composites. *J. Mech. Des.* **130**, 052304 (2008).

50. L. Howell, *Compliant Mechanisms* (Wiley, 2001).

51. C. J. Pennycuick, A wind-tunnel study of gliding flight in the pigeon *Columba Livia*. *J. Exp. Biol.* **49**, 509–526 (1968).

52. A. Vidyasagar, J.-C. Zufferey, D. Floreano, M. Kovač, Performance analysis of jump-gliding locomotion for miniature robotics. *Bioinspir. Biomim.* **10**, 025006 (2015).

53. M. A. Woodward, M. Sitti, MultiMo-Bat: A biologically inspired integrated jumping–gliding robot. *Int. J. Robot. Res.* **33**, 1511–1529 (2014).

54. R. Zufferey, A. Ortega Ancel, A. Farinha, R. Siddall, S. F. Armanini, M. Nasr, R. V. Brahmal, G. Kennedy, M. Kovac, Consecutive aquatic jump-gliding with water-reactive fuel. *Sci. Robot.* **4**, eaax7330 (2019).

55. A. L. Desbiens, M. T. Pope, D. L. Christensen, E. W. Hawkes, M. R. Cutkosky, Design principles for efficient, repeated jumpgliding. *Bioinspir. Biomim.* **9**, 025009 (2014).

56. M. Ilton, M. S. Bhamla, X. Ma, S. M. Cox, L. L. Fitchett, Y. Kim, J.-s. Koh, D. Krishnamurthy, C.-Y. Kuo, F. Z. Temel, A. J. Crosby, M. Prakash, G. P. Sutton, R. J. Wood, E. Azizi, S. Bergbreiter, S. N. Patek, The principles of cascading power limits in small, fast biological and engineered systems. *Science* **360**, eaao1082 (2018).

57. M. Alexander, *Principles of Animal Locomotion* (Princeton Univ. Press, 2003).

58. M. Kovac, M. Fuchs, A. Guignard, J. C. Zufferey, D. Floreano, A miniature 7g jumping robot, in *Proceedings of the 2008 IEEE International Conference on Robotics and Automation*, Pasadena, CA, 19 to 23 May 2008 (IEEE, 2008), pp. 373–378.

59. J. Zhao, J. Xu, B. Gao, N. Xi, F. J. Cintron, M. W. Mutka, L. Xiao, MSU jumper: A single-motor-actuated miniature steerable jumping robot. *IEEE Trans. Robot.* **29**, 602–614 (2013).

60. M. Noh, S.-W. Kim, S. An, J.-S. Koh, K.-J. Cho, Flea-inspired catapult mechanism for miniature jumping robots. *IEEE Trans. Robot.* **28**, 1007–1018 (2012).

61. J.-S. Koh, E. Yang, G.-P. Jung, S.-P. Jung, J. H. Son, S.-I. Lee, P. G. Jablonski, R. J. Wood, H.-Y. Kim, K.-J. Cho, Jumping on water: Surface tension–dominated jumping of water striders and robotic insects. *Science* **349**, 517–521 (2015).

62. D. W. Haldane, M. M. Plecnik, J. K. Yim, R. S. Fearing, Robotic vertical jumping agility via series-elastic power modulation. *Sci. Robot.* **1**, eaag2048 (2016).

63. H. C. Bennet-Clark, The energetics of the jump of the locust *Schistocerca gregaria*. *J. Exp. Biol.* **63**, 53–83 (1975).

64. C. Wan, Z. Hao, X. Feng, Structures, properties, and energy-storage mechanisms of the semi-lunar process cuticles in locusts. *Sci. Rep.* **6**, 35219 (2016).

Citation: S.-M. Baek, S. Yim, S.-H. Chae, D.-Y. Lee, K.-J. Cho, Ladybird beetle–inspired compliant origami. *Sci. Robot.* **5**, eaaz6262 (2020).

Science Robotics

Ladybird beetle–inspired compliant origami

Sang-Min Baek, Sojung Yim, Soo-Hwan Chae, Dae-Young Lee and Kyu-Jin Cho

ARTICLE TOOLS	http://robotics.sciencemag.org/content/5/41/eaaz6262
SUPPLEMENTARY MATERIALS	http://robotics.sciencemag.org/content/suppl/2020/04/13/5.41.eaaz6262.DC1
RELATED CONTENT	http://robotics.sciencemag.org/content/robotics/4/36/eaay3493.full http://robotics.sciencemag.org/content/robotics/4/33/eaax7020.full http://robotics.sciencemag.org/content/robotics/3/16/eaar2915.full http://robotics.sciencemag.org/content/robotics/6/53/eabe0201.full http://robotics.sciencemag.org/content/robotics/6/53/eabf5116.full http://robotics.sciencemag.org/content/robotics/6/53/eabe0637.full
REFERENCES	This article cites 52 articles, 14 of which you can access for free http://robotics.sciencemag.org/content/5/41/eaaz6262#BIBL
PERMISSIONS	http://www.sciencemag.org/help/reprints-and-permissions

Use of this article is subject to the Terms of Service